

18p CUTOFF LONG-WAVELENGTH $\text{In}_x\text{Ga}_{1-x}\text{As}/\text{GaAs}$ QUANTUM-WELL INFRARED PHOTODETECTORS

S. D. Gunapala^a, K. M. S. V. Bandara^b, B. F. Levine^b, J. S. Parka, T. L. Lin^a, J. K. Liua and W. T. Pike^a

a) Center for Space Microelectronics Technology, Jet Propulsion Laboratory, California Institute of Technology, Pasadena CA 91109

b) AT&T Bell Laboratories, Murray Hill, NJ 07974

ABSTRACT

We demonstrate the first longest-wavelength quantum-well infrared photodetector using non lattice-matched $\text{In}_x\text{Ga}_{1-x}\text{As}/\text{GaAs}$ materials system. The defectivity has been found to be comparable to those achieved with the usual lattice-matched $\text{GaAs}/\text{Al}_x\text{Ga}_{1-x}\text{As}$ detectors.

1 INTRODUCTION

There has been a lot of interest recently in the detection of long wavelength ($\lambda = 8-12 \mu\text{m}$) infrared radiation using multiple quantum wells, due to the fact that these quantum-well infrared photodetectors (QWIPs) (1-12) can be fabricated using the mature III-V materials growth and processing technologies. This superior materials control results in high uniformity and thus allows fabrication of large staring arrays ($\lambda = 8-12 \mu\text{m}$) with excellent imaging performance (13-15). Many advanced NASA satellite missions will require long-wavelength infrared (IR) instruments up to a 19 μm cutoff. Examples include the Atmospheric IR Sounder (AIRS) and the Tropospheric Emission Spectrometer (TES) which are being planned for NASA's Earth Observing System (EOS). These space applications have placed stringent requirements on the performance of the IR detectors and arrays including high defectivity, low dark current, uniformity, radiation hardness and lower power dissipation. In addition, the IR spectrum is rich in information vital to the understanding of composition, structure and the energy balance of molecular clouds and stars forming regions of our galaxy. Therefore, NASA has great interest in infrared detectors both inside and outside the atmospheric windows. This paper will present a study and development of a low-dark-current very long-wavelength $\text{In}_x\text{Ga}_{1-x}\text{As}/\text{GaAs}$ QWIPs.

2 QWIP STRUCTURES

For all of the GaAs based QWIPs which have been demonstrated thus far, GaAs is the low bandgap well material and the barriers are lattice matched $\text{Al}_x\text{Ga}_{1-x}\text{As}$, $\text{Ga}_{0.5}\text{In}_{0.5}\text{P}$ or $\text{Al}_{0.5}\text{In}_{0.5}\text{P}$. However, it is interesting to consider GaAs as the barrier material since the transport in binary GaAs is expected to be superior to that of a ternary alloy, as was previously found to be the case in the $\text{In}_{0.53}\text{Ga}_{0.47}\text{As}/\text{InP}$ binary barrier structures (4,5). To achieve this for very long wavelength (12 -18 μm) QWIPs, we have used the lower bandgap non-lattice matched alloy $\text{In}_x\text{Ga}_{1-x}\text{As}$. It has been demonstrated (16,17) that for $x < 0.15$ excellent quality strained layer heterostructures can be grown; thus two QWIPs having the composition $\text{In}_{0.15}\text{Ga}_{0.85}\text{As}$ were grown by molecular beam epitaxy (MBE) and investigated. The first structure shown in Fig. 1 consisted of 5 sets of 80 \AA

$\text{In}_{0.15}\text{Ga}_{0.85}\text{As}$ quantum wells doped $N_D = 5 \times 10^{17} \text{ cm}^{-3}$ separated by 500 Å barriers of undoped GaAs, with the top and bottom contacts being $N_D = 1 \times 10^{18} \text{ cm}^{-3}$ doped GaAs. It should be noted that unlike all the other QWIPs demonstrated thus far, in this structure the heavily doped contacts are made using the *high* bandgap (i.e. GaAs) semiconductor. This is quite different from the GaAs/ $\text{Al}_x\text{Ga}_{1-x}\text{As}$ heterosystem in which the GaAs is the low bandgap quantum well and contact material. This reversal for the $\text{In}_{0.15}\text{Ga}_{0.85}\text{As}/\text{GaAs}$ structure is necessary since a thick contact layer of the strained non-lattice matched $\text{In}_{0.15}\text{Ga}_{0.85}\text{As}$ material would have too many defects and threading dislocations. The design shown in Fig. 1 overcomes this problem by making use of the strong band bending between the heavily doped GaAs contact layers and the first and last $\text{In}_{0.15}\text{Ga}_{0.85}\text{As}$ quantum wells. This results in a large tunneling current (schematically indicated by the double arrow in Fig. 1), which essentially “short circuits” the first and last wells, thus effectively contacting the low bandgap material. The active QWIP structure therefore consists of the central three quantum wells.

The second structure (Fig. 2) is slightly different from the first structure shown in Fig. 1 which consists of 3 sets of 85 Å $\text{In}_{0.15}\text{Ga}_{0.85}\text{As}$ quantum wells doped $N_D = 1 \times 10^{17} \text{ cm}^{-3}$ separated by four 500 Å barriers of undoped GaAs, with the top and bottom contacts being $N_D = 1 \times 10^{17} \text{ cm}^{-3}$ doped GaAs. It is worth noting that unlike the first structure, this structure has two additional undoped GaAs spacer layers between the quantum-wells and the top and bottom contact layers. Due to the undoped spacer layers and the lower contact doping, the tunneling injection current from contacts to the quantum-wells should be significantly smaller in this structure in comparison to the first structure. Therefore the dark current of this device structure should be significantly smaller than the dark current of the previous device structure (and hence have higher defectivity D^*).

III. DARK CURRENT

In order to measure the temperature dependent current-voltage characteristics, 200 μm diameter QWIP mesas were fabricated using wet chemical etching and the results of the first and the second structures are shown in Fig. 3 and Fig. 4 respectively. Note the asymmetry in the dark current (18) with I_D being larger for positive bias (i.e. mesa top positive) than for negative bias. This is due to the asymmetrical growth of $\text{In}_x\text{Ga}_{1-x}\text{As}/\text{GaAs}$ and $\text{GaAs}/\text{In}_x\text{Ga}_{1-x}\text{As}$ interfaces. It should be noted that, even though the second sample has a slightly higher cutoff wavelength than the first structure, Fig. 3 and Fig. 4 clearly show the dark current of the second structure is many orders of magnitude smaller than the dark current of the first structure for temperatures up to 60 K. This clearly indicates that the undoped spacer layers and the lower contact doping significantly reduced the tunneling injection current to the quantum-wells and hence reduced the device dark current as expected. As a result, the second structure is background-limited at a much higher temperature than the first structure.

IV. RESPONSIVITY

The responsivity spectrums of the first and the second samples are shown in Fig. 5 and Fig. 6. The absolute responsivities of the detectors were measured using a calibrated blackbody source. The responsivity spectrum of the first sample has a peak at $\lambda_p = 15.3 \mu\text{m}$ and a cutoff wavelength of $\lambda_c = 18.3 \mu\text{m}$. Thus, the spectral bandwidth is extremely wide $\Delta\lambda / \lambda = 50\%$. The responsivity of the second sample peaks at

slightly higher wavelength $\lambda_p = 18 \mu\text{m}$ and cutoff (half maximum) $\lambda_c = 18.3 \mu\text{m}$ which is determined by the GaAs substrate absorption (i.e. the actual cutoff is $\lambda_c = 20 \mu\text{m}$). The higher peak wavelength $\lambda_p = 18 \mu\text{m}$ of the second sample is attributed to the slightly higher well width. These responsivity peaks are in good agreement with theoretical estimates based on the $\text{In}_{0.15}\text{Ga}_{0.85}\text{As}/\text{GaAs}$ band offset, and even longer wavelength QWIPs can be designed by reducing the In concentration (and thinning the GaAs substrate to reduce its absorption). The peak responsivities of the first and the second samples are 300 and 63 mA/W respectively at bias $V_B = 100 \text{ mV}$.

The measured absolute responsivities (Fig. 7 and Fig. 8) of both samples increase nearly linearly with the bias reaching $R_p = 500$ and 151 mA/W for the first and the second device structures respectively. As shown in Fig. 9 the measured optical gains are also very large for both device structures. The measured optical gains of the first and the second structures reached 10.5 and 8.5 respectively at $V_B = 220 \text{ mV}$, which correspond to very small capture Probabilities (19) (3.2% and 3.9% respectively). This excellent hot-electron transport may be a result of the high mobility binary GaAs barriers.

V. DEFECTIVITY

The noise current in these detectors was measured as a function of bias voltage at various temperatures using a spectrum analyzer. The peak defectivity D^* can now be calculated from $D^* = R \sqrt{A \Delta f} / i_n$, where A is the area of the detector and $A = 3.14 \times 10^{-4} \text{ cm}^2$. Table 1 shows the D^* values of both device structures at various temperatures at bias $V_B = 100 \text{ mV}$. Defectivity D^* of the first device structure was unable to calculate at $T = 50 \text{ K}$ due to the higher dark current. The defectivity values in the Table 1 clearly shows the advantage of the undoped spacer layer which tremendously reduces the dark current (and hence higher defectivity).

TABLE I. Comparison of detectivities with and without undoped spacer layers.

T (K)	D^* ($\text{cm}\sqrt{\text{Hz/W}}$) no spacer layer	D^* ($\text{cm}\sqrt{\text{Hz/W}}$) with spacer layer
10	8.0×10^9	9.7×10^{10}
30	7.8×10^7	2.1×10^9
40	4.0×10^7	1.1×10^9
50		1.3×10^8

VI. SUMMARY

In summary, we have demonstrated the first very long-wavelength ($\lambda_c = 20 \mu\text{m}$) $\text{In}_x\text{Ga}_{1-x}\text{As}/\text{GaAs}$ QWIP. The large responsivity and defectivity D^* values are comparable to those achieved with the usual lattice-matched GaAs/ $\text{Al}_x\text{Ga}_{1-x}\text{As}$ materials system. The very high optical gains and the smaller carrier capture probabilities demonstrates the excellent carrier transport of the GaAs barriers and the potential of this heterobarrier system for very long-wavelength ($\lambda > 14 \mu\text{m}$) QWIPs.

ACKNOWLEDGMENTS

We are grateful to C. A. **Kukkonen**, V. **Sarohia**, S. **Khanna**, K. M. **Koliwad**, B. A. Wilson, and P. J. **Grunthaler** of the Jet Propulsion Laboratory for encouragement and support of this work. The research described in this paper was performed by the Center for Space Microelectronics Technology, Jet Propulsion Laboratory, California Institute of **Technology**, and was jointly sponsored by the Ballistic Missile Defense Organization/Innovative Science and Technology Office, and the National Aeronautics and Space Administration, Office of Advanced Concepts and Technology.

REFERENCES

1. B. F. Levine, C. G. Bethea, G. Hasnain, J. Walker, and R. J. **Malik**, *Appl. Phys. Lett.* 53.(1988) 296.
2. B. F. Levine, *Proceedings of the NATO Advanced Research Workshop on . . ., Intersubband Transitions in Quantum Wells*, **Cargese**, France Sept. 9-14, 1991, edited by E. **Rosencher**, B. **Vinter**, and B. F. Levine (Plenum, London, 1992).
3. J. Y. Andersson and L. **Lundqvist**, *Appl. Phys. Lett.* 59,857 (1991).
4. S. D. **Gunapala**, B. F. Levine, D. **Ritter**, R. A. Harem, and M. B. **Panish**, *Appl. Phys. Lett.* 58,2024 (1991).
5. S. D. **Gunapala**, B. F. Levine, D. **Ritter**, R. A. Harem, and M. B. **Panish**, *Appl. Phys. Lett.* 60,636 (1992).
6. B. K. **Janousek**, M. J. **Daugherty**, W. L. **Bloss**, M. L. **Rosenbluth**, M. J. **O'Loughlin**, H. **Kanter**, F. J. De **Luccia**, and L. E. **Perry**, *J. Appl. Phys.* 67,7608 (1990).
7. S. R. Andrews and B. A. Miller, *J. Appl. Phys.* 70,993 (1991).
8. L. S. **Yu** and S. S. Li, *Appl. Phys. Lett.* 59,1332 (1991).
9. A. G. Steele, H. C. Liu, M. Buchanan, and Z. R. **Wasilewski**, *Appl. Phys. Lett.* 59, 3625 (1991).
10. S. D. **Gunapala**, B. F. Levine, L. **Pfeiffer**, and K. **West**, *J. Appl. Phys.* 69, 6517 (1990).
11. M. J. Kane S. **Millidge**, M. T. Emeny, D. Lee, D. R.P. Guy, and C. R. Whitehouse in Ref. 2.
12. C. S. Wu, C. P. Wen, R. N. Sate, M. Hu, C. W. Tu, J. **Zhang**, L. D. **Flesner**, L. **Pham**, and P. S. **Nayer**, *IEEE Tran. Electron Devices* 39,234 (1992),
13. B. F. Levine, C. G. **Bethea**, K. G. **Glogovsky**, J. W. **Stayt**, and R. E. **Labenguth**, *Semicon. Sci. Technol.* 6 (1991) cl 14.

14. M. T. **Asom** et al., Proceedings of the **IRIS** Specialty Group on Infrared Materials, Boulder, CO, August 12-16,1991, Vol. I, p. 13.
15. L. J. **Kozlowski**, G. M. Williams, G. J. Sullivan, C. W. **Farley**, R. J. Anderson, J. K. **Chen**, D. T. **Cheung**, W. E. **Tennant**, and R. E. **DeWames**, IEEE Trans. Electron Devices 38,1124 (1991).
16. **X. Zhou**, P. **K. Bhattacharya**, G. Hugo, S. C. Hong and E. **Gulari**, Appl. Phys. Lett-54,855 (1989).
17. B. **Elman**, E. S. **Koteles**, P. **Melman**, C. **Jagannath**, J. **Lee** and D. **Dugger**, Appl. Phys. **Lett.** 55,1659 (1989).
18. A **Zussman**, B. F. **Levine**, J. M. **KUO** and J. de **Jong**, J. Appl. Phys. **70**,5101(1991).
19. The well capture probabilities (P_c) were calculated from $g = 1/NP_c$, where N is the number of quantum wells.

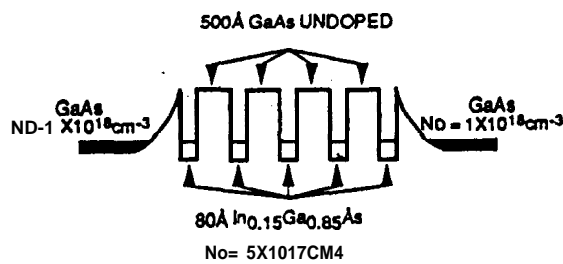


Fig. 1 Conduction-band diagram of the first $\text{In}_{0.15}\text{Ga}_{0.85}\text{As}/\text{GaAs}$ QWIP structure.

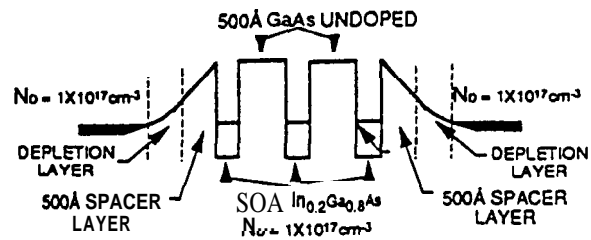


Fig. 2 Conduction-band diagram of the second $\text{In}_{0.15}\text{Ga}_{0.85}\text{As}/\text{GaAs}$ QWIP structure. Unlike the first structure, this structure has two additional undoped GaAs spacer layers between the quantum-wells and the top and bottom contact layers.

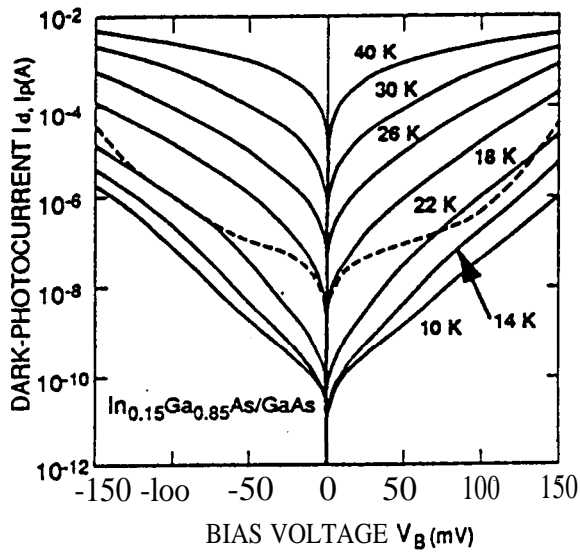


Fig. 3 Dark current versus bias voltage at various temperatures for the first device structure. The dashed curve shows the 300 K window photo-current.

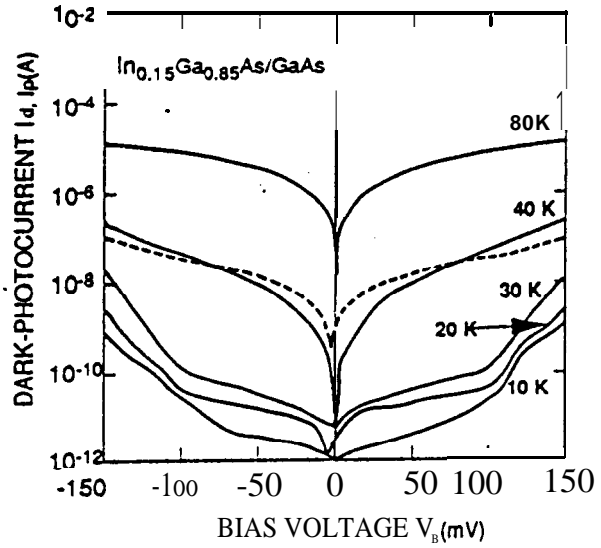


Fig. 4 Dark current versus bias voltage at various temperatures for the second device structure. The dashed curve shows the 300 K window photo-current. It should be noted that this device is background limited at much higher temperature than the previous device.

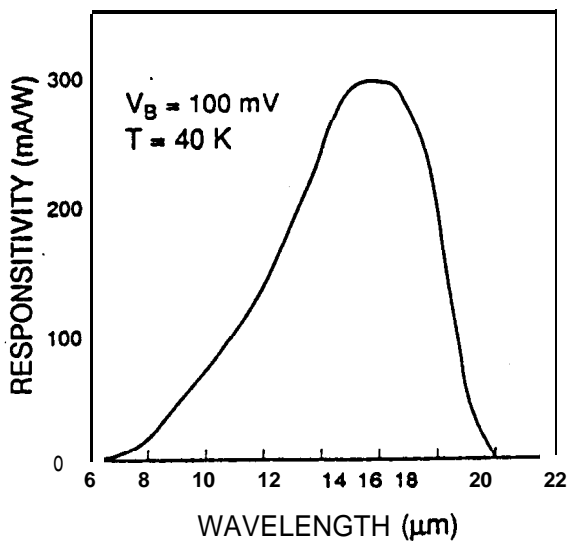


Fig. 5 Responsivity spectrum of the first sample measured at $T = 40$ K.

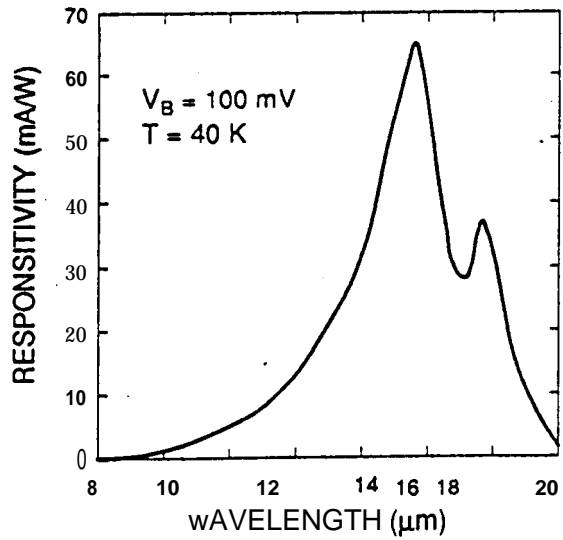


Fig. 6 Responsivity spectrum of the second sample measured at $T = 40$ K.

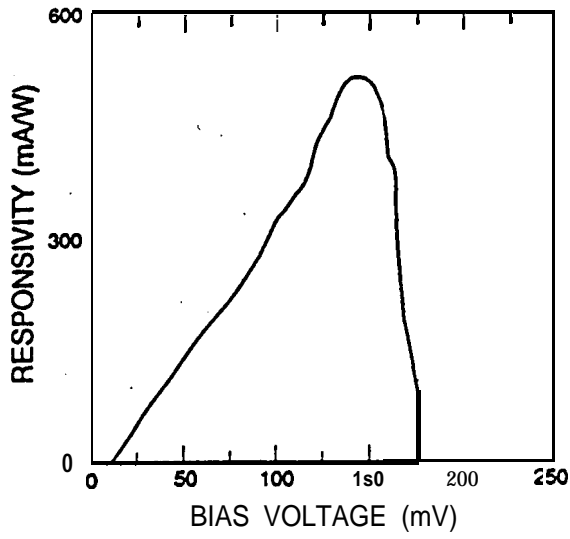


Fig. 7 Bias dependent **peak responsivity** of the first sample measured at $T = 40$ K.

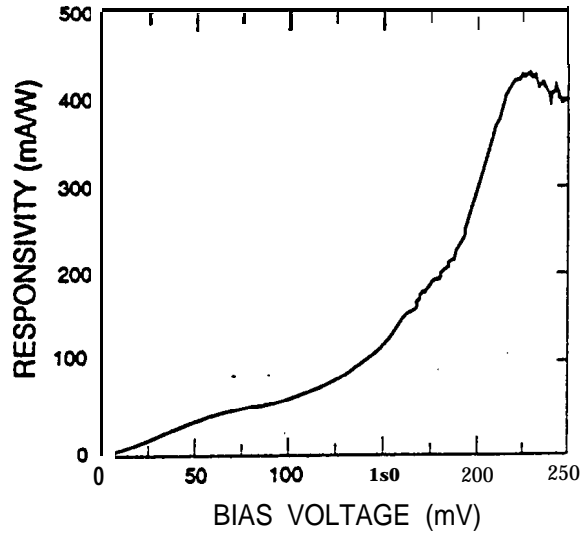


Fig. 8 Bias dependent **peak responsivity** of the second sample measured at $T = 40$ K.

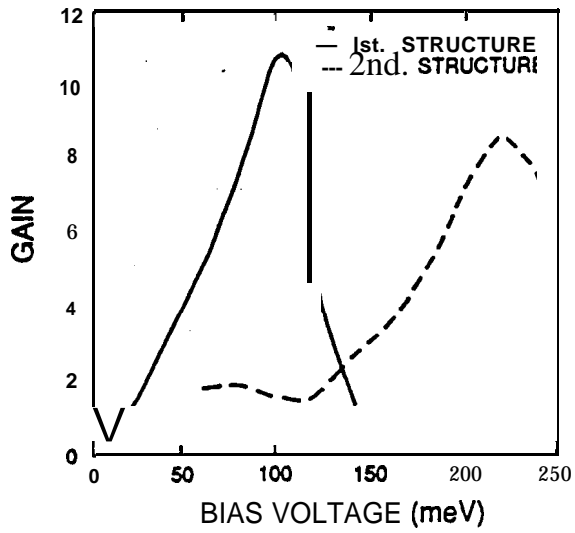


Fig. 9 Optical gain versus bias voltage for both device structures at temperature $T = 40$ K.